The Canadian Mineralogist
Vol. 36, pp. 741-754 (1998)

FIBROUS CHLORITE AND MUSCOVITE FROM THE KAISERSBERG GRAPHITE MINE, STYRIA, AUSTRIA

JOHANN G. RAITH [1]

Institute of Geological Sciences, University of Leoben, A-8700 Leoben, Austria

HOJATOLLAH VALI [1]

Electron Microscopy Center, McGill University, 3640 University Street, Montreal, Quebec H3A 2B2

Abstract

Phyllosilicates with unusual elongate platy to fibrous morphology occur at the Kaisersberg graphite mine, Styria, Austria, in Upper Carboniferous graphite schists of the Eastern Greywacke Zone. A detailed mineralogical investigation revealed that these aggregates of fibrous minerals consist of Mg–Fe-bearing chlorite (polytype IIb) and alkali-deficient muscovite (predominantly of $2M_1$ polytype). They occur as intergrowths with graphite (graphite-d_{1A} type; "semi-graphite") and in thin synmetamorphic veins in graphitic schists. The chlorite ($0.52 < X_{Mg} < 0.68$) is associated with quartz, muscovite, graphite and accessory rutile, pyrite, chalcopyrite, and ullmannite. In chlorite-poor assemblages, chloritoid ($0.08 < X_{Mg} < 0.26$) and kyanite are important minerals. Formation of this low-grade metamorphic assemblage is related to Alpine regional metamorphism, which reached lower greenschist-facies conditions (*ca.* 360–410°C, minimum pressure *ca.* 2 kbar) at Kaisersberg. The semi-graphitic nature of the carbonaceous material is confirmed by reflectance and XRD measurements.

Keywords: asbestos, chlorite, alkali-deficient muscovite, graphite, Kaisersberg, Styria, Austria.

Sommaire

Nous décrivons des phyllosilicates ayant une morphologie allongée en plaquettes, voire même asbestiforme, dans la mine de graphite de Kaisersberg, en Styrie, Autriche, dans des schistes graphitiques d'âge carbonifère de la zone orientale des grauwackes. D'après une étude minéralogique détaillée, ces agrégats fibreux contiennent une chlorite Mg–Fe (polytype IIb) et une muscovite déficitaire en alcalins (le polytype $2M_1$ surtout). Ceux-ci sont en intercroissance avec le graphite, de type d_{1A} ou "semi-graphite", en veinules étroites dans les schistes graphitiques. La chlorite ($0.52 < X_{Mg} < 0.68$) est associée au quartz, à la muscovite, au graphite et aux accessoires rutile, pyrite, chalcopyrite, et ullmannite. Dans les assemblages à faible teneur en chlorite, chloritoïde ($0.08 < X_{Mg} < 0.26$) et kyanite sont plus importants. La formation de cet assemblage typique d'un métamorphisme de faible intensité serait liée à l'événement alpin, qui a atteint le faciès schistes-verts inférieur (environ 360–410°C, pression minimum environ 2 kbar) à Kaisersberg. Des mesures de réflectance et de diffraction X confirment la nature semi-graphitique de la fraction carbonée.

(Traduit par la Rédaction)

Mots-clés: asbestos, chlorite, muscovite déficitaire en alcalins, graphite, Kaisersberg, Styrie, Autriche.

[1] *E-mail address*: raith@unileoben.ac.at, vali_h@geosci.lan.mcgill.ca

Introduction

Asbestiform minerals are recognized as a serious health hazard. Because of their physical and chemical properties, their industrial use is now severely restricted in modern society. The even minor occurrence of asbestiform minerals in various raw materials and industrial products, from where they could be liberated during mining, processing or usage, is one aspect of this concern.

Mineral aggregates with an acicular to asbestiform habit in hand specimen occur in the graphite mine at Kaisersberg, Styria, Austria. They were previously identified as "asbestos" or "hornblende asbestos", but are here recognized as chlorite and muscovite. It is our aim in this paper to clarify the geological occurrence, the mineralogical composition and the processes of formation of these minerals by means of optical microscopy, X-ray-diffraction (XRD), scanning (SEM) and transmission electron microscopy (TEM), electron microprobe (EMP), Fourier-transform infrared spectroscopy (FTIR), thermal analysis, reflectivity measurements on carbonaceous material and phase-equilibrium relations.

Geological Setting

The mine at Kaisersberg (Fig. 1) exploits a major deposit of graphite in Austria. In 1996, its annual production was 7316 t (raw, milled and flotated graphite; unpublished data, Oberste Bergbehörde, 1996). It is one of several stratabound deposits of graphite in the Eastern Greywacke Zone, occurring in Upper Carboniferous strata of the Veitsch nappe (Holzer 1966, Scharfe 1981). This nappe is tectonically the deepest of the Austro-alpine Greywacke Zone; it tectonically overlies a medium-grade metamorphic suite and Permo-Mesozoic cover sequences (Ratschbacher 1984, Nievoll 1984, Neubauer & Vozárová 1989, Ebner *et al.* 1991, Neubauer *et al.* 1994).

The graphite deposits are hosted by a carbonate–clastic sequence (the so-called Sunk Formation), a coarsening-upward sequence characterized by cyclic sedimentation (Ratschbacher 1984, 1985). These 50- to 150-m-thick sequences of graphitic schists, meta-argillites, and metaconglomerates are interpreted as delta to coastal plain sediments. Plant fossils confirm a Westphalian A–C age for this formation.

At Sunk, another important deposit located *ca.* 45 km northwest of Kaisersberg (Fig. 1), polyphase deformation has been documented (Ratschbacher 1985). Regional metamorphism in this part of the Veitsch nappe reached low-grade (epizonal) conditions and has been dated at 53–98 Ma by conventional K–Ar techniques (Ratschbacher & Klima 1985). No details about the structural and metamorphic evolution and the mineral assemblages of the Kaisersberg deposit have been published thus far.

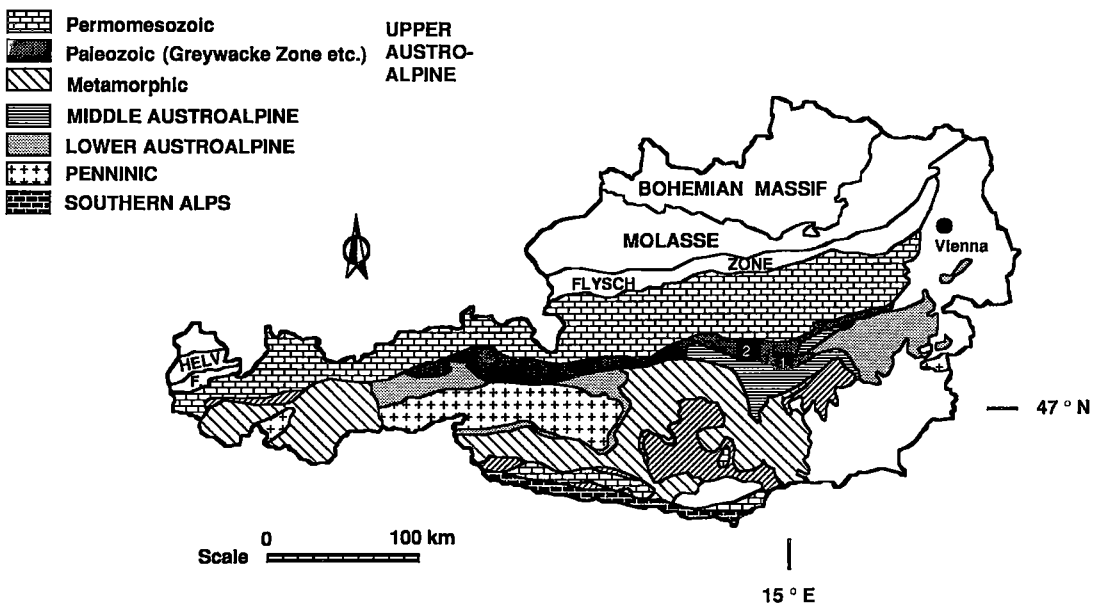

FIG. 1. Simplified geological map of Austria (after Frank 1987) showing the location of the two major graphite deposits, Kaisersberg (1) and Sunk (2), in the Paleozoic Eastern Greywacke zone.

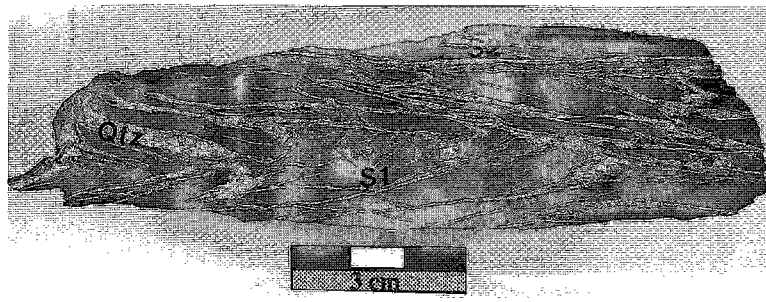

FIG. 2a. Synmetamorphic veins and phyllosilicate-rich layers (light), containing elongate platy to asbestiform muscovite, quartz (Qtz) and only microscopically visible chloritoid and kyanite in graphite schist (dark). Some of the veins and phyllosilicate layers define an early *S*1 foliation, which is folded by tight *F*2 folds, and sheared by a corresponding *S*2 axial plane foliation. Mica-rich layers are reoriented into *S*2 foliation planes. Sample K7. Kaisersberg graphite mine, "Marienbau" underground workings.

PETROGRAPHY

Samples K1 to K3 represent material provided from mineral collections of the first author and the Institute of Geological Sciences, University of Leoben, respectively. Other samples (K5, K7, K19, K20, K23) were collected from the "Marienbau" underground workings.

The macroscopic aggregates of acicular to fibrous minerals occur in strongly deformed graphitic schists, which preserve, in analogy to the Sunk deposit (Ratschbacher 1985), evidence of two major events of deformation. The aggregates occur (a) as fine-grained intergrowths in graphite, (b) in concordant veins mm to cm thick, and (c) in discordant, stockwork-like veinlets. Concordant quartz – phyllosilicate veins formed coevally with the first phase of deformation (*D*1, platy cleavage) as well as during *D*2. The *S*1 phyllosilicate – graphite layers and early quartz veins were folded by *F*2 folds and sheared by a corresponding *S*2 axial plane foliation (Fig. 2a). Fibrous phyllosilicates crystallized during *D*2, are extremely elongate, and define a mineral lineation (*L*2). Discordant veins of quartz developed in local extensional structures that formed syn- to late *D*2 (Fig. 2b).

Microscopically elongate crystals of phyllosilicate show perfect parallel orientation. Intercalated polycrystalline quartz grains are also elongate owing to ductile deformation and evidence postkinematic recrystallization (*e.g.*, 120° triple junctions, straight grain-boundaries). Single fibers of phyllosilicate attain several cm in length, with a length-to-width (L/W) ratio much greater than 3. The diameter of individual fibers is <3–10 μm. Microscopically, these fibers are identified as either chlorite or muscovite. In hand specimen, chlorite is distinguished by its definite greenish color, whereas muscovite has a waxy or silky luster and white color (Fig. 2a). Chlorite and quartz are the major minerals in sample K1, with minor muscovite and graphite, and rutile and opaque phases as the accessory minerals. The opaque minerals were identified as pyrite, chalcopyrite and ullmannite. In thin section, the chlorite is colorless and shows normal

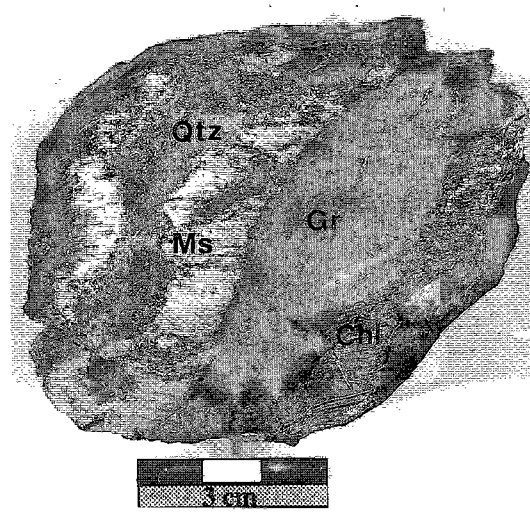

FIG. 2b. Asbestiform chlorite (Chl) and muscovite (Ms) – quartz (Qtz) in discordant extensional veins in finely crystalline graphite (Gr). Kaisersberg graphite mine. Sample courtesy of Prof. Dr. W. Prochaska.

yellowish to greyish first-order interference-colors under crossed polars. In other samples (K2, K3, K19), muscovite and quartz are dominant, with chloritoid, graphite, ± kyanite, ± chlorite as minor minerals. Chloritoid is present as: (a) subhedral to euhedral porphyroblasts up to 0.5 mm across, overgrowing the mica matrix, (b) small (10–50 μm) tabular crystals arranged in star-shaped aggregates in the microcrystalline graphite matrix, and (c) large (up to 0.2 mm) crystals coexisting with kyanite, quartz, ± chlorite in synmetamorphic veins. The crystallization of chloritoid and kyanite is syn- to late *D*2 and partly outlasted penetrative *D*2 deformation. A kaolinite-group mineral, detected by electron microprobe only, formed by replacement of kyanite.

Analytical Methods

X-ray diffractometry was performed using a Philips PW3710 diffractometer (analyst: F. Seidl). Three quartz-poor, powdered, random mounts (K1–K3) were analyzed under the following operating conditions: Cu$K\alpha$ radiation, 50 kV, 20 mA, goniometer velocity 1/2°/minute, divergence slit 1/2°, receiving slit 0.1 mm, scatter slit 1/2°. The crystallinity of the carbonaceous matter was studied on oriented, HF-treated samples according to the method of Landis (1991).

The minerals were analyzed with a wavelength-dispersion ARL–SEMQ electron microprobe, using the program MacQuant 5/2 96 and natural minerals (kaersutite, biotite) as standards and the following operating conditions: carbon coating, 15 kV, 20 nA, modified Bence & Albee matrix correction model. Some samples were re-analyzed and selectively examined with a JEOL 6310 SEM with an integrated Oxford energy-dispersion (EDX) system (carbon coating, natural mineral standards, sample current 2 nA, counting time 100 s, and ZAF matrix correction) at the Institute of Mineralogy, Crystallography and Petrology, University of Graz.

The FTIR spectra of muscovite were measured in polyoil immersion at the Institute of Mineralogy and Crystallography, University of Vienna, (analyst: A. Beran, Vienna) using a Perkin Elmer 1760X FTIR spectrometer. Thermal analysis (DTA) was kindly provided by Netzsch Gerätebau (Selb, Germany) and done with a NETZSCH–STA 409 instrument under the following conditions: range 25–1400°C, heating rate 5 K/minute, air, static sample-holder, Thermogravimeter (TG) – Differential Scanning Calorimeter (DSC) type, Pt crucible. Monomineralic muscovite powder was used for both techniques.

The fibrous minerals and their association with the matrix were studied with a Cambridge scanning electron microscope (SEM) from fracture surfaces of fragments collected from the original samples and coated with Au–Pd. The layer structures of mica and chlorite phases were examined with high-resolution transmission electron microscopy (HRTEM). Powdered samples of mica and chlorite were embedded in a low-viscosity, thermally curing epoxy resin. Ultrathin sections (70–80 nm) were cut from the blocks of resin with a diamond knife and transferred to 300 mesh, formvar-coated Cu TEM grids. To investigate possible alteration and mixed-layer structures, the grids containing the ultrathin sections were treated directly with a dilute solution of octadecylamine hydrochloride (Vali & Hesse 1990). This technique enables the identification of layer sequences with variable charge-distribution and the direct imaging of the stacking order of discrete components of the layer silicate (Vali *et al.* 1994).

The growth characteristics and surface morphology of chlorite and mica were studied from platinum–carbon (Pt–C) replicas in conventional TEM (CTEM). Replicas are prepared by the condensation of heavy metals (*e.g.*, Au, Ag, and Pt) on as grown, cleavage, or fractured surfaces. This "decoration and shadowing" technique enables the investigation of the surface morphology of crystals at a resolution near 1 nm. The SEM is conventionally used to investigate morphological features of crystalline material. The limits of resolution of the SEM, however, do not permit the detection of microtopographical and morphological features at a very fine scale. CTEM investigation of replicas offers the unique opportunity to correlate microtopographic features on crystal surfaces with the corresponding internal microfabric observed in ultrathin sections at the same TEM scale. Careful interpretation of replicas can provide significant information on the evolution of crystal growth.

Fragments of the original fibrous chlorite and mica crystals were carefully mounted on a flat substrate and transferred to the freeze–fracture unit (Balzers BAF 310). The surface of the crystals were shadowed with a thin Pt–C film (1.5 nm thick) and subsequently coated by a supporting carbon film (10–15 nm thick). The replica was cleaned by dissolving the fibers adhering to the replica with 6% HF solution, rinsed with deionized H_2O and transferred to 300 mesh TEM grids. CTEM imaging at Scherzer defocus was performed with a JEOL FX 2000 equipped with an energy-dispersion X-ray detector and at an accelerating voltage of 100 kV. The reflectivity of the carbonaceous material was measured with a Zeiss MPM–400 photometer (PHOTAN program, min-max mode) at a wavelength of 546 nm in oil (Zeiss immersion oil 518 C; $n_e = 1.518$; 23°C) on polished sections under polarized light. Approximately 50 to 70 measurements were performed on each sample.

Diffractometry

Standard powder XRD analyses revealed that sample K1 is predominantly chlorite with minor quartz and muscovite, whereas K2 and K3 are muscovite-dominated samples containing small amounts of chlorite, chloritoid and quartz.

The *chlorite* is a trioctahedral 14-Å chlorite with random Mg–Fe distribution in the octahedrally co-ordinated position, as deduced from the intensity ratios of the uneven basal reflections. According to the criteria of Bailey (1980, p. 91), it is classified as polytype IIb. The *muscovite* shows diagnostic peaks of dioctahedral mica and is mainly of the $2M_1$ polytype. Semiquantitative calculations of the ratio $2M_1/1M_d$, made by comparing the intensity of the (023) peak at 3.74 Å with that at ~2.58 Å (method of Velde & Hower 1963), also show the predominance of the $2M_1$ polytype. Samples K2 and K3 have *ca.* 10% and 30% 1*M* muscovite, respectively. Muscovite is well ordered and shows sharp reflections.

The d_{002} of carbonaceous material, measured at maximum intensity, is 3.40 ± 0.01 Å (mean, single standard deviation of five measurements). The d_{002} value at 1/3 peak height is 3.41 ± 0.01 Å. The full width-half maximum (FWHM) is 2.19 ± 0.53° 2θ. The material studied is thus clearly classified as graphite-d_{1A} according to Landis (1971).

Chemical Composition of the Minerals

Mineral formulae were calculated from EMP and quantitative SEM data on a water-free basis assuming 22 atoms of oxygen per formula unit (*apfu*) for muscovite, 28 for chlorite, and 12 for chloritoid. Representative compositions are listed in Table 1.

The grains of *chlorite* in the three samples analyzed are relatively homogeneous. Si in the *T* position varies between 5.00 and 5.53 *apfu*, and X_{Mg} [= Mg/(Mg + Fe^{2+}) on a molar basis], between 0.52 and 0.68. In sample K1, the mean proportion of Si is 5.08 ± 0.06 *apfu*, and the mean X_{Mg} is 0.61 ± 0.02 (n = 11). Alkali, Ti, Mn, and Ca contents are below the detection limit. Chlorite is thus chemically classified as a Mg–Fe chlorite (ripidolite).

Chloritoid was analyzed in two samples (K2, K19), and the cations given below are calculated on the basis of 12 *apfu* of oxygen. In sample K2, where chloritoid is present in a mica matrix, Si is 1.92 to 2.11 *apfu*, Al 3.79 to 4.16 *apfu*; in sample K19, where it occurs in synmetamorphic veins together with quartz and kyanite, Si is 2.01–2.05 *apfu* and Al is 3.95–3.99 *apfu*. Manganese contents are generally low and vary between 0.1 to 0.6 wt.% MnO. X_{Mg} ranges between 0.08 and 0.18 (mean 0.15 ± 0.03, n = 7) in sample K2, and between 0.24 and 0.26 (mean 0.25 ± 0.01, n = 8) in K19. Chloritoid, enclosed by the fine-grained graphite (K2 1/4), has a X_{Mg} of 0.08.

Muscovite analyzed in samples K2, K3, K7, and K19 show minor chemical variation. Silica varies between 5.97 to 6.52 *apfu*, with the sum of cations in the octahedral position between 4.13 and 4.29. The sum of the divalent (M^{2+}) cations Mg, Fe (total Fe as Fe^{2+}) and Mn ranges between 0.08 and 0.19 *apfu*. Owing to the Al/Si ratios and low M^{2+} contents, the mica is classified as muscovite. The deficiency in the *A* position, however, is obvious (Table 1). The sum of K, Na, and Ca which, on the basis of 22 atoms of oxygen, should be 2 in the ideal mica structure, ranges between 0.80 and 1.52 *apfu*. Na varies from 0.08 to 0.31 *apfu*. Mica inclusions in graphite are higher in Na and Ca (up to 0.45 Na, up to 0.15 Ca), but also are alkali-deficient.

Possible explanations for the low alkali contents of muscovite could be: (a) analytical problems (*e.g.*, alkali loss during analysis), (b) the presence of molecules of H_2O or of H_3O^+ (Loucks 1991), which cannot be recognized by EMP techniques, (c) interlayering of muscovite and another alkali-free layer silicate or graphite, or (d) alternatively, this position could show considerable vacancies.

TABLE 1. COMPOSITION OF CHLORITE, MUSCOVITE AND CHLORITOID FROM THE KAISERSBERG GRAPHITE DEPOSIT, STYRIA, AUSTRIA

Sample No.	K1	K2	K7	K2	K2	K3	K7	K19	K2	K3	K7	K19
Anal. No.	1/1	2/4B	2/6E	1/3	3/7E	2/2	2/5E	2/2E	1/4	1/1	2/4E	2/3E
Mineral	Chl	Chl	Chl	Ms	Ms	Ms	Ms	Ms	Cld	Cld	Cld	Cld
SiO_2 wt.%	24.74	24.21	26.36	47.61	49.54	46.99	49.08	47.81	23.58	24.84	24.79	24.68
TiO_2	0.00	0.05	0.04	0.57	0.33	0.06	0.09	0.14	0.18	0.00	0.00	0.13
Al_2O_3	24.70	23.18	24.06	39.28	36.99	37.68	38.41	36.97	43.31	40.53	40.98	40.91
FeO	20.23	23.17	17.56	0.34	0.42	0.63	0.37	0.55	25.45	27.01	20.79	20.80
MnO	0.04	0.02	0.02	0.00	0.00	0.02	0.00	0.00	0.12	0.38	0.41	0.41
MgO	17.79	13.97	18.95	0.24	0.64	0.44	0.36	0.60	1.21	2.52	4.10	3.90
CaO	0.00	0.06	0.05	0.85	0.04	0.00	0.00	0.07	0.07	0.00	0.03	0.00
Na_2O	0.03	0.18	0.10	1.79	0.43	0.81	0.65	0.62	0.00	0.04	0.12	0.21
K_2O	0.01	0.03	0.02	3.49	6.68	5.28	6.34	7.65	0.00	0.02	0.03	0.04
Total	87.54	84.87	87.16	94.17	95.07	91.91	95.30	94.41	93.92	95.34	91.25	91.08
Si *apfu*	5.069	5.216	5.332	6.124	6.374	6.226	6.288	6.257	1.922	2.014	2.037	2.033
Ti	0.000	0.008	0.006	0.055	0.032	0.006	0.009	0.014	0.011	0.000	0.000	0.008
Al	5.965	5.886	5.736	5.955	5.609	5.884	5.800	5.703	4.159	3.872	3.969	3.972
Fe^{2+}	3.466	4.175	2.970	0.037	0.045	0.070	0.040	0.060	1.734	1.831	1.429	1.433
Mn	0.007	0.004	0.003	0.000	0.000	0.002	0.000	0.000	0.008	0.026	0.029	0.029
Mg	5.434	4.487	5.714	0.046	0.123	0.087	0.069	0.117	0.147	0.304	0.502	0.479
Ca	0.000	0.014	0.011	0.117	0.006	0.000	0.000	0.010	0.006	0.000	0.003	0.000
Na	0.012	0.075	0.039	0.447	0.107	0.208	0.161	0.157	0.000	0.006	0.019	0.034
K	0.003	0.008	0.005	0.573	1.096	0.892	1.036	1.277	0.000	0.002	0.003	0.004
ΣCations	19.955	19.874	19.817	13.353	13.392	13.375	13.402	13.595	7.987	8.055	7.990	7.992
oxygen atoms	28	28	28	22	22	22	22	22	12	12	12	12
mg	61.06	51.80	65.80	55.42	73.09	55.41	63.43	66.04	7.82	14.24	26.01	25.05
^{IV}Al	2.931	2.780	2.668	1.876	1.626	1.774	1.712	1.743				
Sum *Y*				4.217	4.183	4.275	4.206	4.151				
Sum *A*				1.137	1.209	1.100	1.197	1.444				
T°C *	409.9	386.3	367.6									

E in analysis number: analysis done by SEM-EDX method; all other compositions were determined by electron-microprobe analysis with wavelength-dispersion spectrometry. ^{IV}Al: tetrahedrally coordinated aluminum; mg: 100*Mg/(Mg + Fe^{2+}). Sum *Y*: sum of cations in the octahedrally coordinated position of the mica. Sum *A*: sum of cations in the interlayer position of the mica. * Temperature calculated of the ^{IV}Al contents of chlorite, according to Cathelineau (1988). Symbols: Chl chlorite, Ms muscovite, Cld chloritoid, *apfu*: atoms per formula unit.

To evaluate the first possibility, the samples examined by wavelength-dispersion microprobe analysis were analyzed with SEM–EDX. Although the latter method revealed higher contents (*ca.* 1–1.5 wt.% K_2O higher, Table 1), total alkali contents are still much lower than in ideal muscovite. As systematic changes of the acquisition time (10–100 s) during EDX analyses did not show major (time-dependent) changes of the count rates of alkalis, alkali loss is judged to be negligible.

Thermal analysis (TG/DTG) and FTIR-spectroscopy were applied to obtain information of possible H_2O content of micas. Thermal analysis shows five TG steps, with weight losses of 0.32, 0.35, 4.15, 0.79 and 0.57%. Maximum weight-losses occur at 89°, 306°, 687° and 972°C. By comparison with the DSC curve, the first TG step, corresponding to an endothermic peak at *ca.* 200°C, is likely caused by the release of adsorbed H_2O (H_2O^-). The second step corresponds to an exothermic peak at 315°C (extrapolated onset at 278°C) and indicates the presence of carbonaceous material (*i.e.*, minor graphite impurities in the sample). The dehydroxylation (*i.e.*, release of OH groups from the mica structure) is correlated with steps 3 and 4 and corresponds to a large endothermic peak (thermal maximum at 652°C). Most importantly, there is *no* indication of the release of molecular H_2O in the sample studied.

From the lack of the H_2O vibration at *ca.* 1635 cm^{-1} in the FTIR spectra, no significant amount of molecular H_2O seems to be present in the muscovite structure. In summary, deficiency in the *A* position of the mica cannot be explained with the presence of molecular H_2O or H_3O^+. As no other cations (*e.g.*, Cs, Ba) were detected, this could either indicate natural vacancies in the muscovite interlayer or interlayering of an alkali-free sheet silicate or graphite with the muscovite.

Electron Microscopy

The SEM and TEM were used to investigate the morphology of fibrous chlorite and muscovite in samples K1 and K3. Chlorite (K1) appears in SEM at low magnification as extremely elongate platy and fibrous crystals (Fig. 3a). At higher magnification (*e.g.*, 1500×; Fig. 3b), aggregates of fibrous chlorite with diameters ranging from one to tens of micrometers seem to have developed by "rolling-in" of platy chlorite. The elongate lath-shaped morphology of muscovite (K3) is recognized at various magnifications (200×, Fig. 3c; 1000× Fig. 3d). Similar to chlorite, these crystals are, however, extremely elongate in one direction and may also show "rolling-in" parallel to their long axis. The extremely fibrous aggregates typical of chlorite have not been observed in the muscovite sample.

FIG. 3a. SEM image of asbestiform chlorite. Extremely elongate platy aggregates (background) and fibrous crystals (foreground) are distinguished. Fiber thickness is *ca.* 10 μm. Scale bar: 50 μm. Sample K1. Kaisersberg graphite mine. b. Detail of *a* showing that the kinked, platy crystallites are bent parallel to their long axis and roll in to form round fibers. Scale bar: 20 μm. Sample K1. Kaisersberg graphite mine. c. Muscovite showing elongate platy crystal morphology. Some aggregates show a beginning stage of bending and "rolling in" parallel to their long axis (right part of photograph, arrow). Scale bar: 200 μm. Sample K3. Kaisersberg graphite mine. d. Muscovite cut perpendicular to (002) showing characteristic cleavage planes (upper half of photograph) and cut subparallel to (002) showing the elongate platy morphology (lower half of photograph). Scale bar: 20 μm. Sample K3. Kaisersberg graphite mine.

Conventional TEM (CTEM) imaging of Pt–C replicas obtained from aggregates of fibrous chlorite and muscovite separated from the original samples show the growth characteristics of these minerals. The surface microtopography of individual fibers of chlorite (Figs. 4a, b) is distinct from that of muscovite (Figs. 4c, d). The surface structures of these minerals, however, are distinct from the common chlorite and muscovite crystals present in igneous and metamorphic rocks (Tomura *et al.* 1979, Sunagawa 1984). In addition to the common cleavage surface perpendicular to the c^* direction, fibrous chlorite and muscovite seem to also have cleavage properties perpendicular to the *a* or *b* axis. There are also distinct differences in the surface morphology of these minerals and illitic material (Vali *et al.* 1991, Kitagawa 1998). Surprisingly, the cleavage surface of fibrous chlorite and muscovite show characteristics of as-grown surfaces, which can be recognized by the fine-scale growth-steps along the long axis of the fibers in Figure 4d. In some cases, the chlorite seems to have more curved edges than the relatively flat muscovite and shows overgrowths of distinct crystal phases (Figs. 4a, b). Characterization of these phases and their association with chlorite have yet to be established.

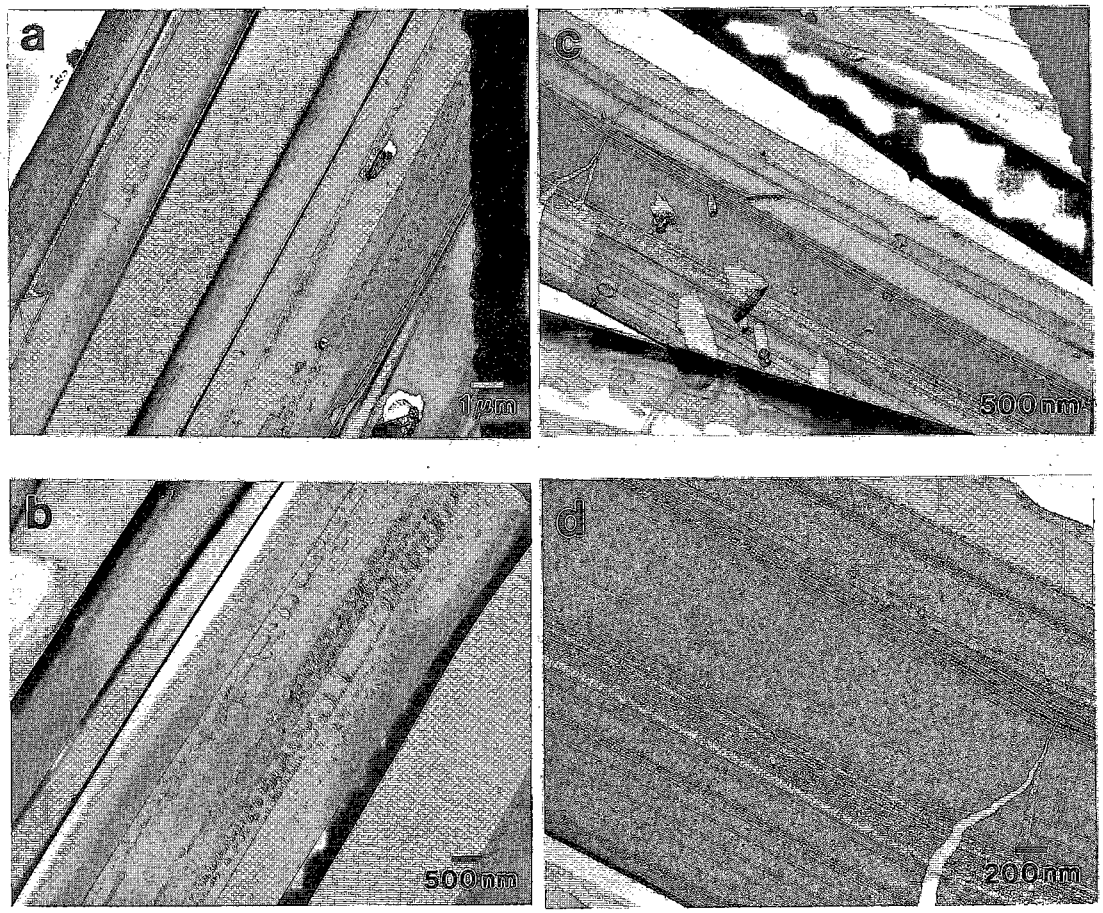

FIG. 4. CTEM images of Pt–C replicas obtained from aggregates of fibrous chlorite and muscovite. Surface microtopography of fibrous chlorite. b. Detail of *a* showing overgrowths of distinct crystal phases. c. Surface microtopography of fibrous muscovite. d. Detail of *b* showing the fine-scale growth steps along the long axis of the fibers.

To correlate the surface morphology with the internal microstructure, lattice fringes and stacking order of silicate layers were investigated in ultrathin sections of powdered chlorite and muscovite samples in HRTEM. Figure 5a represents a typical cross-section through the fibers of muscovite (*i.e.*, parallel to the c* direction) (Fig. 5b). Stacks of packets are observed consisting of coherent sequences of 2:1 layer silicates having 1 nm spacing. The overall dimensions of these packets correspond to the size of the individual fibers observed in Pt–C replicas shown in Figures 4c and d. No structural defects, bending or "rolling-in" features were observed.

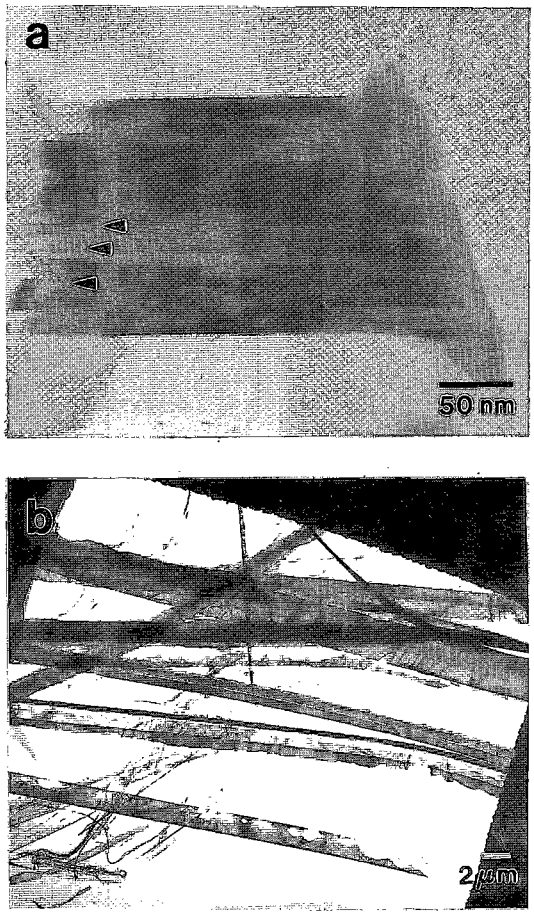

FIG. 5. TEM images of asbestiform muscovite. a. HRTEM image showing stacks of packets of muscovite after exchange with a solution of octadecylamine hydrochloride. The coherent sequences of 2:1 layers have a layer spacing of 1 nm. No expanded interlayers are present, suggesting that the muscovite has not been altered. Scale bar: 50 nm. Arrows show individual packets of muscovite. b. CTEM image of lath-shaped fibers of muscovite. Scale bar: 2 µm.

Preliminary results of the *n*-alkylammonium cation-exchanged samples (see analytical methods) revealed no expansion of interlayers within the packets of muscovite. This suggests that the muscovite has not been altered, and that its structure is distinct from that of illite, which shows an interstratification of expanded and non-expanded interlayers after long-chain alkylammonium cation-exchange. Since the chemical composition of the muscovite reveals a deficit in K in the interlayer sites, partial expansion of the interlayer was expected (Vali *et al.* 1994). Further investigation is required to fully explore the true nature of this material. Examination of the internal structure of the chlorite also is in progress.

Reflectance of Organic Material

The measured values of R_{min} and R_{max} of five samples of graphite and the calculated means and standard deviations are given in Figure 6.

R_{max} is definitely lower and R_{min} higher than in perfectly ordered graphite [$15.6 < R_{max} < 17.8\%$, $0.2 < R_{min} < 0.8\%$; data from several authors (Teichmüller 1987, p. 158, and references therein)]. Coarsely crystalline (crystal size from 50 to 500 µm) carbonaceous material (*e.g.*, sample K20) gives slightly lower R_{max} values than smaller crystallites (<50 µm) of the same sample. In general, R_{min} shows a much larger sample-dependent variation compared to R_{max}. This is largely the effect of the orientation of crystallites within the sample in relation to the polished surface (*i.e.*, sections cut perpendicular to the cleavage planes show maximum bireflectance and the lowest R_{min} values, and those with crystallites oriented subparallel to S1 or S2 cleavage planes show much higher values) (see histograms, Fig. 6).

The observed R_{max} and R_{min} range is characteristic of "transitional material" (Diessel *et al.* 1978) or, using another classification, of "semi-graphite" (Teichmüller 1987). The high bireflectance indicates a rank definitely above the meta-anthracite stage. These data, considered in light of XRD findings, preclude the presence of perfectly ordered graphite.

Discussion

Comparison with typical asbestiform minerals

The term *asbestos* comprises several amphibole- and serpentine-group minerals, all showing extremely fibrous to asbestiform morphology of crystals. For any of these minerals to be considered asbestos, the length of single fibers has to be >5 µm, the diameter, <5 µm, and the length:diameter ratio must be >3 according to the U. S. Occupational Safety and Health Administration (Ross 1985). Typical asbestos minerals are either amphiboles or the chrysotile form of serpentine [$Mg_3Si_2O_5(OH)_4$]. Amphibole asbestos includes asbestiform varieties of grunerite ("amosite") [$Fe^{2+},Mg)_7Si_8O_{22}(OH)_2$], riebeckite ("crocidolite")

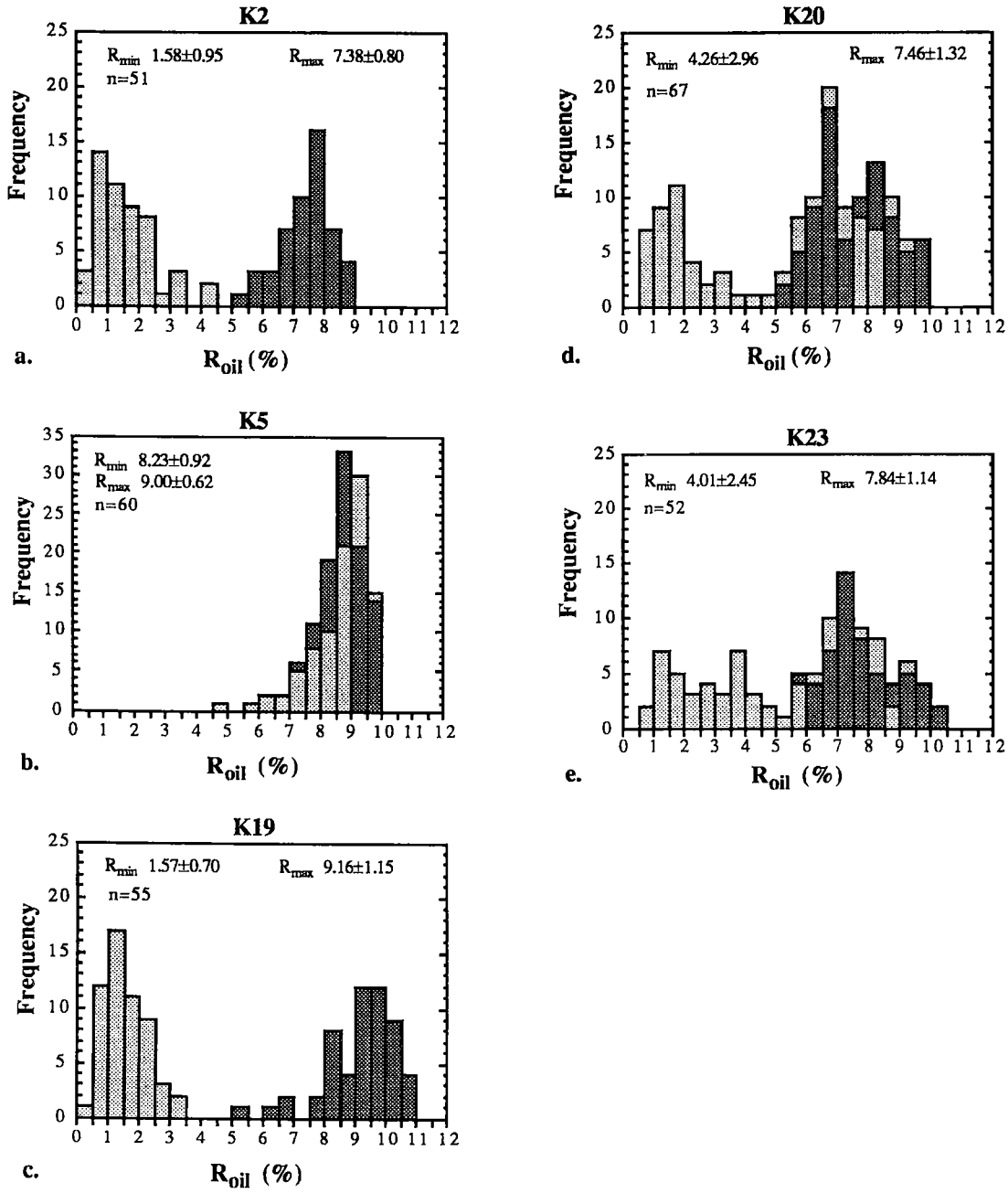

FIG. 6. Reflectance measurements (R_{max}, R_{min}) of graphite shown in histograms. Means and standard deviations of *n* measurements are given.

$[Na_2(Fe^{2+},Mg)_3Fe^{3+}{}_2Si_8O_{22}(OH)_2]$, and calcic amphiboles of the tremolite – actinolite series $[Ca_2(Mg,Fe^{2+})_5Si_8O_{22}(OH)_2]$, as well as anthophyllite $[(Mg,Fe^{2+})_7Si_8O_{22}(OH)_2]$ (Ross 1985).

The fibrous minerals from Kaisersberg have been identified as Mg–Fe chlorite and muscovite in this study. Thus they are certainly atypical asbestiform minerals. With respect to their morphology, however, they

partly fulfil the criteria as given above. SEM and TEM images show that individual "fibers" commonly are formed from extremely elongate platy crystals. The bending and "rolling-in" of these platy aggregates parallel to the long axis can, especially with chlorite, result in the formation of a true fibrous morphology. The internal structure, and to some extent, the surface topography of our samples, are more similar to asbestiform amphiboles rather than to chrysotile. Physical grinding of amphiboles, however, results in dispersion of large particles into extremely fine fibers, whereas grinding of fibrous mica and chlorite results in extremely fine cleavage fragments with no fibrous characteristics.

Processes of formation

The formation of fibrous chlorite and muscovite during regional metamorphic processes is deduced from the following observations. These minerals (a) occur in synmetamorphic veins in graphite schists whose formation is strongly controlled by the stress field during regional metamorphism, and (b) are associated with quartz, graphite, ± chloritoid, ± kyanite, all minerals that show typical metamorphic textures (*e.g.*, quartz recrystallization, perfect orientation of phyllosilicates). Fibrous chlorite and muscovite are part of the peak metamorphic assemblage and are newly crystallized. There is no petrographic evidence (*e.g.*, relics) that chlorite and muscovite formed by replacement of chrysotile or amphiboles, a hypothesis proposed by Weninger (1966).

In contrast, kaolinite-group minerals formed by replacement of kyanite; the formation of dickite, associated with galena, sphalerite, pyrite and chalcopyrite in a 30- to 50-cm-thick quartz vein (Schroll & Spatzek 1984) could correspond to a retrograde stage of metamorphism.

Maximum P–T conditions of 200–250°C and 1.5 to 1.8 kbar, (*i.e.*, anchizonal metamorphic conditions) were proposed for mineral formation (Schroll & Spatzek 1984, and references therein). Considering the following criteria, however, these P–T estimates seem too low.

(1) Though chloritoid has occasionally been reported from anchizonal metasedimentary rocks, it normally forms during low-grade metamorphism (Frey 1987, p. 54–55). Its association with muscovite, quartz, kyanite ± chlorite in synmetamorphic veins and the lack of pyrophyllite support this interpretation (see below).

(2) Muscovite consists mainly of the $2M_1$ polytype. The structural change from muscovite $1M$ to $2M_1$ depends on metamorphic grade, especially on temperature. Experimental studies demonstrate that above 200 to 350°C, at a $P(H_2O)$ of 2 kbar, $2M_1$ is the stable polytype (Frey 1987). Thus, the transition from the $1M$ or $1Md$ to the $2M_1$ polytype should be largely complete in the epizone.

(3) The observed structural ordering of carbonaceous material and its classification as disordered graphite (graphite-d_{1A}) suggest P–T conditions above those of the anchizone (*e.g.*, see Fig. 10 in Itaya 1981). This classification as "semi-graphite" is also supported by reflectivity measurements of graphite.

(4) Muscovite is well ordered and shows sharp (00*l*) reflections in the XRD spectra. This confirms regional data on illite crystallinity in the Eastern Greywacke Zone (Ratschbacher & Klima 1985, Kralik *et al.* 1987).

A better quantitative estimation of the metamorphic P–T conditions may be obtained by considering mineral stabilities in combination with chlorite geothermometry. As stated above, kyanite (± chloritoid) is stable in synmetamorphic quartz veins, and pyrophyllite is absent. In the simple Al_2O_3–SiO_2–H_2O (ASH) system, the univariant dehydration reaction,

$$\text{pyrophyllite} = \text{kyanite} + \text{quartz} + H_2O$$

has been calculated using THERMOCALC (Powell & Holland 1988; Fig. 7); it lies between *ca.* 370 to 400°C for pressures between 2 to 5 kbar and $X(H_2O) = 1.0$. A minimum temperature of *ca.* 370°C is deduced from the presence of kyanite, which is only stable above 2 kbar for the H_2O-saturated case. The position of this dehydration reaction in P–T space is, however, strongly affected by the activity of H_2O. Non-aqueous fluids such as CH_4 or CO_2 commonly exist with graphite under metamorphic conditions (Barrenechea *et al.* 1997) and could reduce the activity of H_2O during metamorphism of graphitic schists, thus, shifting this univariant reaction to lower temperatures. The reaction was calculated for varying values of $X(H_2O)$ (Fig. 7).

The empirically calibrated chlorite thermometer of Cathelineau (1988), based on the Tschermaks exchange in chlorite, gives temperatures between 335 and 420°C. The mean temperature is 408 ± 10°C ($n = 11$; Table 1) in sample K1, 361°C ($n = 2$) in sample K2, and 372°C ($n = 2$) in sample K7, and this mean temperature range is shown in Figure 7. These data confirm that epizonal P–T conditions were reached at the Kaisersberg graphite deposit during Alpine regional metamorphism.

Conclusions

Chlorite and muscovite showing unusual elongate platy, acicular to fibrous morphology, and previously referred to as "asbestos" or "hornblende asbestos", occur in the matrix and in syn- to late metamorphic quartz veins of graphite schists at the Kaisersberg graphite mine. SEM and TEM imaging revealed that these mineral aggregates partly show fibrous textures and developed by "rolling-in" of extremely, elongate platy or tabular crystals parallel to their long axis. A Mg–Fe chlorite and alkali-deficient muscovite are associated with quartz, chloritoid, kyanite, rutile and accessory sulfides and formed during regional metamorphism of Alpine age. Metamorphism transformed Carboniferous coal seams to mineable deposits of graphite at low-grade conditions (*ca.* 360–410°C, >2.0 kbar).

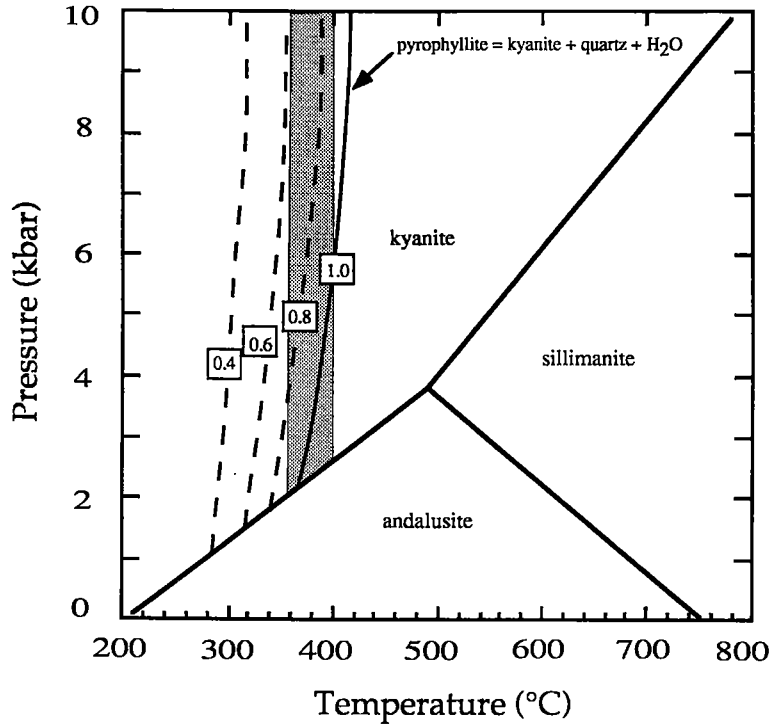

FIG. 7. P–T estimates of mineral assemblages from the Kaisersberg graphite mine. Metamorphic temperatures of 360–400°C are estimated from the reaction pyrophyllite = kyanite + quartz + H_2O and results of chlorite geothermometry (stippled field). In view of the presence of kyanite, pressures are inferred to have been greater than 2 kbar. The effect of a decrease in $X(H_2O)$ on the position of the dehydration reaction in P–T space (dashed lines) for various values of $X(H_2O)$, as given in boxes, also is shown. Reactions were calculated with the program THERMOCALC (Powell & Holland 1988).

ACKNOWLEDGEMENTS

We are grateful to the following, who contributed to this study in various ways: Mr. F. Seidl and Prof. Dr. W. Vortisch (Division of Prospecting and Applied Sedimentology, University of Leoben) for part of the XRD analyses; G. Hawranek and Prof. Dr. F. Jeglitsch (Department of Physical Metallurgy and Material Testing, University of Leoben) for SEM imaging; H. Mühlhans for assistance with EMP analyses with the SEMQ microprobe; Dr. W. Prochaska for assistance with sample preparation; Drs. F. Melcher and G. Rantitsch for critically reading the manuscript; Dr. C. Hauzenberger and Prof. Dr. H. Hoinkes (Institute of Mineralogy, Crystallography and Petrology, University of Graz) for assistance with and offering access to the JEOL SEM at their department; Prof. Dr. A. Beran (Institute of Mineralogy and Crystallography, University of Vienna) performed the FTIR spectrometry. Netzsch Gerätebau Ltd., Selb, Germany, kindly provided the thermal analysis. Dr. R.F. Martin is thanked for initiating collaboration with the Electron Microscopy Center, McGill University, Montreal and his editorial handling of the manuscript. Finally, I thank Dipl. Ing. W. Twrdy, the manager of the graphite mine at Kaisersberg, for access to the underground workings.

REFERENCES

BAILEY, S.W. (1980): Structures of layer silicates. *In* Crystal Structures of Clay Minerals and their X-ray Identification (G.W. Brindley & G. Brown, eds.). *Mineral. Soc., Monogr.* **5**, 2-123.

BARRENECHEA, J.F., LUQUE, J.F., RODAS, M. & PASTERIS, J.D. (1997): Vein-type graphite in Jurassic volcanic rocks of the External Zone of the Betic Cordillera, southern Spain. *Can. Mineral.* **35**, 1379-1390.

CATHELINEAU, M. (1988): Cation site occupancy in chlorites and illites as a function of temperature. *Clay Mineral.* **23**, 471-485.

DIESSEL, C.F.K., BROTHERS, R.N. & BLACK, P.M. (1978): Coalification and graphitization in high-pressure schists in New Caledonia. *Contrib. Mineral. Petrol.* **68**, 63-78.

EBNER, F., KOVÁCS, S. & SCHÖNLAUB, H. P. (1991): Das klassische Karbon in Österreich und Ungarn – ein Vergleich der sedimentären fossilführenden Vorkommen. *In* Jubiläumsschrift 20 Jahre Geologische Zusammenarbeit Österreich – Ungarn 1 (H. Lobitzer & G. Csásár, eds). (263-294).

FRANK, W. (1987): Evolution of the Austrolapine elements in the Cretaceous. *In* Geodynamics of the Eastern Alps (H. W. Flügel & P. Faupl, eds.). Franz Deuticke, Vienna, Austria (379-406).

FREY, M. (1987): Very low-grade metamorphism of clastic sedimentary rocks. *In* Low Temperature Metamorphism (M. Frey, ed.). Blackie, Glasgow, U.K. (9-58).

HOLZER, H. (1966): Bericht 1965 über lagerstättenkundliche Arbeiten, Graphit. *Verh. Geol. B.-A.* **1966**, A62-A63.

ITAYA, T. (1981): Carbonaceous material in pelitic schists of the Sanbagawa metamorphic belt in central Shikoku, Japan. *Lithos* **14**, 215-224.

KITAGAWA, R. (1998): Surface microtopography of illite crystals. *Can. Mineral.* **37** (in press).

KRALIK, M., KRUMM, H. & SCHRAMM, J.M. (1987): Low grade and very low grade metamorphism in the Northern Calcareous Alps and in the Greywacke Zone: illite-crystallinity data and isotopic ages. *In* Geodynamics of the Eastern Alps (H.W. Flügel & P. Faupl, eds). Deutike, Vienna, Austria (164-178).

LANDIS, C.A. (1971): Graphitization of dispersed carbonaceous material in metamorphic rocks. *Contrib. Mineral. Petrol.* **30**, 34-45.

LOUCKS, R.R. (1991): The bound-interlayer H_2O content of potassic white micas: muscovite – hydromuscovite – hydrophyllite solutions. *Am. Mineral.* **76**, 1563-1579.

NEUBAUER, F., HANDLER, R., HERMANN, S. & PAULUS, G. (1994): Revised lithostratigraphy and structure of the Eastern Greywacke Zone (Eastern Alps). *Mitt. Österr. Geol. Ges.* **86** (1993), 61-74.

_____ & VOZÁROVÁ, A. (1989): The Noetsch – Veitsch – North Gemeric zone of Alps and Carpathians: correlation, paleogeography and significance for Variscan orogeny. *In* Thirty Years of Geological Cooperation Between Austria and Czechoslovakia (D. Manarikova & H. Lobitzer, eds.). Vydal Ustred. Ustav. Geol., Prague, Czechoslovakia (167-171).

NIEVOLL, J. (1984): Der Südrand der Grauwackenzone zwischen Stübming und Neuberg (Obersteiermark, ÖK 103 Kindberg). *Mitt. Österr. Geol. Ges.* **77**, 63-71.

POWELL, R. & HOLLAND, T.J.B. (1988): An internally consistent dataset with uncertainties and correlations. 3. Applications to geobarometry, worked examples and a computer program. *J. Metamorphic Geol.* **6**, 173-204.

RATSCHBACHER, L. (1984): Beitrag zur Neugliederung der Veitscher Decke (Grauwackenzone) in ihrem Westabschnitt (Obersteiermark, Österreich). *Jb. Geol. B.-A.* **127**, 423-453.

_____ (1985): Strukturgeologische Grundlagenforschungsaspekte als Prospektions- und Abbaurichtlinien am Beispiel Graphitbergbau Sunk/Trieben (Paltental, Steiermark). *Arch. f. Lagerst. Forsch. Geol. B.-A.* **6**, 81-84.

_____ & KLIMA, K. (1985): Übersicht über Geologie und Mineralgehalt in einem Querprofil von Altkristallin zur Kalkalpenbasis (Triebener Tauernpaß - Flitzenschlucht, Paltental, Steiermark, Österreich). *Jb. Geol. B.-A.* **128**, 151-173.

ROSS, M. (1985): The geologic occurrences and health hazards of amphibole and serpentine asbestos. *In* Amphiboles and Other Hydrous Pyriboles – Mineralogy (D.R. Veblen, ed.). *Rev. Mineral.* **9A**, 279-323.

SCHARFE, G. (1981): Steirische Graphitvorkommen. *Mitt. Abt. Geol. Paläont. Bergb. Landesmuseum Joanneum* **42**, 117-121.

SCHROLL, E. & SPATZEK, H. (1984): Dickit und eine Mikroerzmineralisation aus dem Graphitbergbau Kaisersberg, Steiermark. *Mitt. Abt. Miner. Landesmuseum Joanneum* **52**, 23-25.

SUNAGAWA, I. (1984): Growth of crystals in nature. *In* Material Science of Earth's Interior (I. Sunagawa, ed.). Terrapub., Tokyo, Japan.

TEICHMÜLLER, M. (1987): Organic material and very low-grade metamorphism. *In* Low Temperature Metamorphism (M. Frey, ed.). Blackie, Glasgow, U.K. (114-161).

TOMURA, S., KITAMURA, M. & SUNAGAWA, I. (1979): Surface microtopography of metamorphic white micas. *Phys. Chem. Minerals* **5**, 65-81.

VALI, H. & HESSE, R. (1990): Alkylammonium ion treatment of clay minerals in ultrathin section; a new method for HRTEM examination of expandable layers. *Am. Mineral.* **75**, 1443-1446.

_____, _____ & KOHLER, E. (1991): Combined freeze-etch replicas and HRTEM imaging as tools to study the fundamental particles and the multiphase nature of 2:1 layer silicates. *Am. Mineral.* **76**, 1973-1984.

_____, _____ & MARTIN, R.F. (1994): A TEM-based definition of 2:1 layer silicates and their interstratified constituents. *Am. Mineral.* **79,** 644-653.

VELDE, B. & HOWER, J. (1963): Petrological significance of illite polymorphism in Paleozoic sedimentary rocks. *Am. Mineral.* **48,** 1239-1254.

WENINGER, M. (1966): *Beiträge zur Geochemie der Grafitlagerstätten der Grauwackenzone mit besonderer Berücksichtigung der Vorkommen von Kaisersberg und Sunk/Trieben.* Ph.D. thesis, Univ. Vienna, Vienna, Austria.

Received December 23, 1996, revised manuscript accepted February 15, 1998.